Phase-Sensitive Single-Pixel THz Imaging Using Intensity-Only Measurements

Syed An Nazmus Saqueb, *Graduate Student Member, IEEE*, and Kubilay Sertel, *Senior Member, IEEE*

***Abstract*—We present a submillimeter-wave phase-sensitive imaging system by using single-pixel, intensity-only measurements. We implement this unique modality by utilizing the photoelectric effect on a high-resistivity silicon wafer illuminated by visible light from a commercial liquid crystal display projector. Randomly distributed mask patterns (16×16 pixel) are generated using two levels of light intensity projected on a high-resistivity silicon wafer. The spatial modulation of the amplitude and phase of the incident terahertz is achieved via the photoelectric effect, resulting in the random modulation of the object beams phase fronts accordingly. Subsequently, intensity-only measurements are collected by using a single-pixel sensor for each of the random mask patterns, and the "Phaselift" algorithm is applied to reconstruct the magnitude and phase of the 16×16 pixel image. We also demonstrate that the phase image of the scene shows superior contrast to the intensity image and offers thickness discernibility of a paper object down to 190 μm at 690 GHz.**

***Index Terms*—Compressed sensing, Phaselift, phase-sensitive, terahertz (THz).**

I. Introduction

PHASE information plays a very important role when it comes to contrast in image formation. Conventional imaging techniques utilize the difference in absorption cross section of the sample to produce the intensity image, and thus often suffer from poor contrast in many practical applications. For example, in biomedical imaging, it is often required to differentiate soft tissues with similar absorption as healthy tissues in mammography for earlier detection of breast cancer. Such malignancies not only have a very small absorption cross section, they also differ very little in this regard from the regular tissue. As a result, the conventional intensity imaging technique produces poor contrast in the formation of the image. In most of these cases, phase shifts introduced on a transmitted signal by the different tissue types can provide enhanced contrast, particularly when shorter electromagnetic wavelengths of the millimeter-wave and submillimeter-wave frequencies are used [1].

Phase-sensitive imaging, enabled by the wave nature of light, reconstructs the phase of the image along with its intensity pattern. This approach not only produces better contrast in the image by computing the phase shift between different structures, as such, it also leads to an improvement in the resolution as a bonus. Many X-ray interferometric techniques such as diffraction enhanced imaging (DEI) and multiple-image radiography (MIR) have been successfully demonstrated in biomedical phase-contrast imaging [2], [3]. However, these methods have strict technical requirements on the sources and detectors. For instance, most need a high-brilliance synchrotron radiation source and have a very small alignment tolerance in the imaging system due to the short wavelength of X-rays. In addition, the ionization effects of X-rays on biomolecules and the associated potential hazard to human health have always been a key concern in the field of biomedical imaging.

Imaging using the terahertz (THz) regime of electromagnetic spectrum has been attracting interest among researchers in the field due to its nonionizing nature as well as the much shorter wavelengths as compared to radio frequencies, potentially enabling much higher resolution. The low energy and high spatial resolution of THz waves have already resulted in many imaging applications such as safe and early detection of cancerous tissues, security screening (detection of illegal weapons and drugs), and nondestructive evaluation in pharmaceuticals [4]–[6]. Nevertheless, there has not been significant progress in miniaturizing efficient sources and low-noise detectors, hence limiting the proliferation of THz imaging instrumentation. Focal plane array imagers demonstrate great potential for real-time THz imaging [7]. However, they depend on high power sources and complex fabrication processes, resulting in a very high cost. A single-pixel raster scanning method eliminates the need of multiple detectors by scanning the object plane pixel by pixel mechanically with a single detector [8]. However, such imagers are rather bulky and suffer from long acquisition time due to the mechanical scanning method. Alternatively, for optical-frequency imaging using single-pixel detectors, spatial modulation of light and compressive sensing (CS) has been demonstrated in [9], wherein spatial modulation is realized using a reflection-mode digital micromirror device (DMD) array. Using a DMD, each micron-sized mirror in the array can be electronically controlled to reflect the object beam toward the detector, resulting in the binary modulation of the image in the mask's plane. In this approach, the source illuminates the object, and the object beam is modulated via a spatial light modulator (SLM) by using a set of independent mask patterns. The modulated beam is focused onto a single detector, and the $N \times N$ image is reconstructed from n consecutive measurements of the beam after a spatial random or Hadamard mask pattern, where $n = N^2$. The number of measurements can be reduced by utilizing CS algorithms, i.e., $m < n$ measurements are sufficient for scenes that contain sparse information.

Manuscript received March 21, 2016; revised August 5, 2016; accepted September 4, 2016. Date of publication October 6, 2016; date of current version November 1, 2016. This work was supported by the NSF Division of Mathematical Sciences under Grant DMS-1322393 under the project "Methods and algorithms from harmonic analysis for threat detection."

The authors are with the Department of Electrical and Computer Engineering, The Ohio State University, Columbus, OH 43212 USA (e-mail: saqueb.1@osu.edu; sertel.1@osu.edu).

Color versions of one or more of the figures in this paper are available online at http://ieeexplore.ieee.org.

Digital Object Identifier 10.1109/TTHZ.2016.2610760

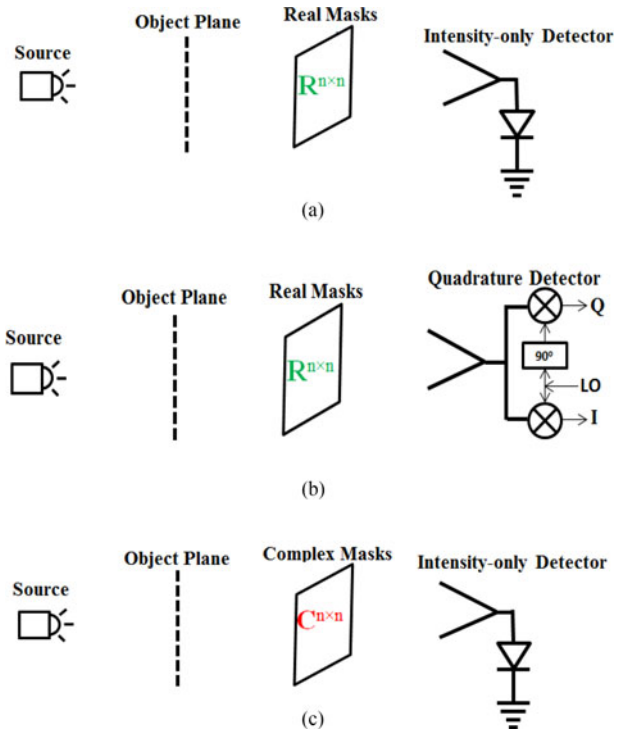

Fig. 1. Alternative single-pixel compressive imaging schemes by using various detector and mask combinations: (a) intensity reconstruction using real-valued masks and real-valued (intensity-only) measurements, (b) complex image reconstruction using real-valued masks and complex (magnitude and phase) measurements, and (c) complex image reconstruction through *Phaselift* using complex-valued masks and intensity-only measurements.

Fig. 1 illustrates the typical alternatives for a transmission mode SLM utilized in the context of CS. Although a DMD array is a simple and fast means of modulation in optical frequencies, the dimension of the mirrors in this device is not suited for much longer wavelengths in the millimeter-wave and submillimeter-wave bands. Several techniques such as metamaterial arrays, liquid crystal devices, and graphene modulator arrays have been demonstrated as alternatives [10]–[12]. Nevertheless, these sophisticated devices are rather costly and rely on complex fabrication processes. Earlier studies suggest the possibility of realizing a fast, high-resolution, and high-performance SLM for submillimeter-wave imaging by exploiting the photoexcitation of the semiconductor surface [13]–[15]. To this end, THz CS imaging using the photoexcitation of a high-resistivity silicon (Si) wafer has been demonstrated [16]–[18]. In this system, amplitude modulating masks (real-valued mask patterns) are formed by projecting computer-generated pixelated patterns on the high-resistivity Si wafer by using a commercial DLP projector and taking the intensity-only measurements (i.e., real-valued measurements) by using a single detector, to reconstruct the intensity of the image, as illustrated in Fig. 1(a). Chan *et al.* [19] computed a CS reconstruction of the phase contrast image of the object by using real masks and recording both the magnitude and the phase of the wave of the detected signal, i.e., complex measurements, as shown in Fig. 1(b). However, in their method, the masks were made of metallic apertures and were mechanically shifted, which renders the system slow.

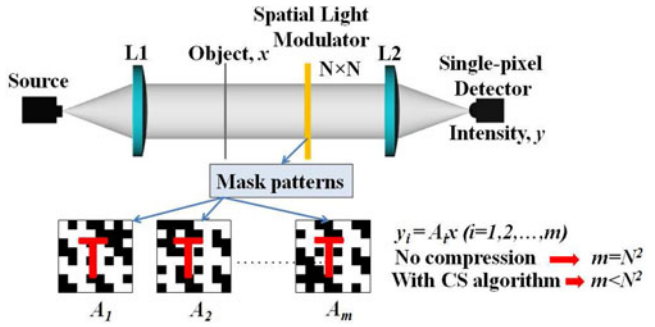

Fig. 2. Illustration of the basic setup for single-pixel compressive imaging. The source is used to illuminate the scene and an SLM is used to scramble the object beam by using random mask patterns. Subsequently, an intensity-only detector samples and records the lowest spatial frequency component for each mask.

Moreover, complex measurements of the received signal require a phase-sensitive detector, significantly increasing the cost of the imaging system.

Recent research in phase retrieval algorithms developed by Candes *et al.* [20] showed that the phase reconstruction of a signal of length n is possible by using $n \log n$ intensity-only measurements collected using complex-valued CS masks. The resulting reconstruction algorithm is termed the *Phaselift* [20]. The unique aspect of the *Phaselift* algorithm is the complex mask patterns that spatially modulate both the magnitude and the phase of the beam, allowing for the reconstruction of the phase information from intensity-only measurements by using a simple detector, as illustrated in Fig. 1(c).

In this work, we present a phase-sensitive submillimeter-wave imaging system exploiting the single-pixel CS imaging technique and the *Phaselift* algorithm. We use optical excitation of high-resistivity silicon to spatially modulate both the amplitude and the phase of the object's THz wave. Binary (i.e., black and white) mask patterns are generated on a computer and projected on the Si wafer by a commercially available liquid crystal display (LCD) projector to control the wavefront modulation. After recording intensity-only measurements of the modulated wave, we employ the *Phaselift* algorithm to recover the phase and amplitude of the image scene. We demonstrate a 16×16 complex image of several object scenes and show the superior contrast of the phase image.

II. Single-Pixel Compressive Imaging and Phaselift

In the single-pixel CS imaging scheme, spatially multiplexed light is detected by a single detector, and the $N \times N$ image is reconstructed from $m < N^2$ number of such measurements. The basic components of this method are a source, focusing lenses, an SLM, and a detector, as shown in Fig. 2. The collimated object beam gets modulated by the SLM, where mask patterns spatially control the transmission of the object wave. Fig. 2 also illustrates several 8×8 binary masks for 64-pixel imaging. Assuming that the dark pixels block the incident wave and the white pixels are transparent, one can define the weight of white and dark pixels as "1" and "0", respectively. After focusing the modulated beam onto the detector, the

measurement y detected by the single-pixel sensor is the lowest spatial frequency component defined by the equation

$$y = \sum_{i=1}^{N^2} a_i x_i \tag{1}$$

where x_i represents the intensity/magnitude of each pixel of an $N \times N$ image and a_i represents the weight of the corresponding pixel in the mask. After collecting m such measurements, one needs to solve the following system of linear equations to obtain the reconstructed intensity image X:

$$[Y] = [A][X] \tag{2}$$

where $[A]$ is an $m \times N^2$ matrix and $[Y]$ is a column vector of length m. One of the challenges in this method is to reduce the number of measurements to enable real-time imaging. Previously, it was shown that a compressible image can be reliably reconstructed from $m < N^2$ random measurements [21]–[23]. To reconstruct both intensity and phase using CS, both the magnitude and the phase of the modulated wave need to be recorded.

Alternatively, the *Phaselift* approach offers recovery of both the intensity and phase from intensity-only measurements, i.e., a complex signal of length n can be reconstructed from m intensity measurements, where m lies between $n \log n$ and $4.5n \log n$ [20]. For an $N \times N$ complex image, the intensity-only measurement y is given by

$$y = \left| \sum_{i=1}^{n} a_i x_i \right|^2 \tag{3}$$

where x_i is the complex value of each pixel, $n = N^2$, and the weight of modulation a_i is complex in this case. The number of measurements m can be kept at the minimum of order O($n \log n$) allowed by the algorithm. Thus, in order for the *Phaselift* algorithm to work, an SLM capable of generating a programmable set of complex-valued masks is needed. To do so in the most cost effective and efficient manner, we utilize the photoelectric effect on semiconductors, as detailed below.

III. Implementation of SLM by Photoexcitation of Silicon

To implement a cost-effective SLM that effectively provides wavefront manipulation of the transmitted signal, we employ the photoconductive property of semiconductors. In particular, the mask patterns are projected onto a Si wafer by using a commercially available LCD projector to generate photoexcited electrons on the surface of the wafer. The photocarriers result in the modulation of the electrical properties of the Si wafer regions that are illuminated by the projected mask pattern. As such, the transmitted THz beam gets spatially modulated according to the distribution of the photoexcited carrier density. In practice, high-resistivity Si is an excellent candidate to implement the complex SLM due to its fairly good transmission characteristic in the THz band. When illuminated with optical energy equal to, or above the band gap of Si (1.12 eV), excess carriers are generated within the penetration depth of the wafer. Under photoexcitation, these carriers contribute to a complex dielectric constant, as given by the Drude model [13], [24]

$$\epsilon = \epsilon_\infty + i\frac{\sigma}{\omega \epsilon_0} \tag{4}$$

where ϵ_∞ is the dielectric constant of the silicon due to the bound electrons and is approximately $\epsilon_\infty \sim 11.7$, ϵ_0 is the free space permittivity, and the conductivity σ is given by

$$\sigma = i\frac{\epsilon_0 \omega_p^2}{\omega + i\Gamma} \tag{5}$$

where Γ is the damping rate, which is the inverse of carrier collision time, and ω_p is the angular plasma frequency defined by

$$\omega_p^2 = \frac{Ne^2}{\epsilon_0 m^*}. \tag{6}$$

In the above, N is the density of carriers, e is the electronic charge, and m^* is the effective mass of electron. Consequently, the transmission characteristics of the photoexcited Si wafer are determined by the plasma frequency in (6). For frequencies above ω_p , the semiconductor acts as a low-loss dielectric. In the absence of photoexcitation, ω_p is well below the THz range in high-resistivity Si as the density of free carriers is very small. In contrast, a large number of free carriers are generated under photoexcitation, for example, given by

$$N_{\text{photo}} = \frac{\alpha \tau I_{\text{ex}}(1-R)}{eh\nu} \tag{7}$$

where τ is the minority carrier lifetime, I_{ex} is the intensity of external light illuminating the wafer, α and R are the absorption coefficient and reflectivity of Si in optical frequency, respectively, h is Planck's constant, and ν is the frequency of incident light.

The excess carriers generated by the optical signal increases the plasma frequency ω_p. For frequencies below ω_p, the photocarriers produce a significant loss in the semiconductor and subsequently attenuate the THz wave. In addition, a phase-shift is also induced on the transmitted wave due to the change in complex refractive index, particularly when ω_p is close to the THz wave's frequency.

The high carrier lifetime in Si makes it possible to achieve plasma frequencies in the order of 1–3 THz by using white light from commercial DLP/LCD projectors. By projecting pixelated patterns on the Si wafer, the amplitude and phase of the transmitted THz wave can thus be spatially modulated and the modulation depth can be further controlled by using grayscale patterns. We should, however, note here that the minimum achievable pixel size is limited by the diffusion length of the carriers in Si, which is in the order of 50–500 μm.

Carrier lifetime τ controls the generation of photocarriers, hence the modulation level for THz transmission. Surface passivation using a quinhydrone–methanol solution notably increases carrier lifetime by reducing the surface recombination velocity [25]. To quantify modulation depth achievable in practice, we considered a 420-μm-thick, 20 000-Ωcm unpassivated wafer and measured a maximum 5 dB amplitude modulation ($|S_{21}|$) of the transmitted THz signal and negligible phase modulation

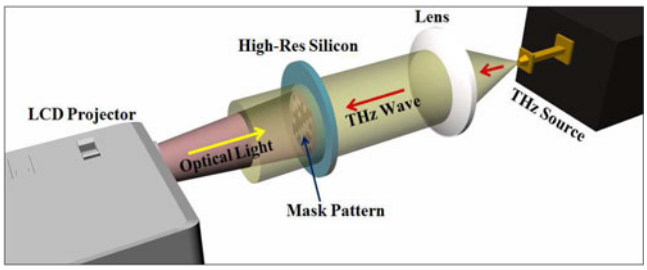

Fig. 3. Illustration of high-resistivity Si wafer photoexcitation to spatially modulate the transmitted THz beam. Computer-generated binary or grayscale patterns are projected on the Si wafer to control the conductivity of each pixel.

at 665 GHz when illuminated with 1 $\mathrm{W/cm^2}$ white light. After treating it with 0.01 $\mathrm{mol/dm^3}$ quinhydrone–methanol solution, the modulation depth was increased up to 15 dB. In addition, a small (5°) phase modulation was also observed at the same frequency. In light of the above observations, this wafer is an excellent candidate for an amplitude-only SLM to generate real-valued masks by projecting binary patterns on the wafer. However, in order to realize a mask with both amplitude and phase modulation, one needs to tune the THz-signal's frequency accordingly. For example, at 690 GHz, amplitude modulation was observed to be around 12 dB and phase modulation around 30°. To further improve the phase modulation depth, Si wafers with different resistivities can be considered. In the following, a 500-μm-thick, 800-Ωcm wafer exhibiting 10 dB of amplitude and 70° of phase modulation was used at 690 GHz.

To generate the complex-valued masks, random binary patterns were focused on the wafer with the aid of a commercial digital LCD projector, as shown in Fig. 3. In these patterns, 0 (white) and 1 (black) are uniformly distributed with equal probability. As noted above, lit pixels produce around 10 dB of amplitude modulation and 70° of phase modulation with respect to dark pixels. Thus, normalizing the weight of the dark pixels as 1, the weight of the lit pixel can be calculated as $0.1 \angle 70^\circ$. Instead of white light, other colors such as red/green/blue can be used for modulation as all three colors, including white light, have energy ($\sim$450–700 nm) higher than the Si bandgap (1100 nm). The level of modulation depends on the intensity of the illumination, absorption coefficient, and reflectivity of Si in the frequency of the color used, as can be seen in (7).

IV. Experimental Procedure

The experimental setup used to demonstrate the *Phaselift* approach is shown in Fig. 4. A pair of vector network analyzer (VNA) frequency extenders (500–750 GHz from Virginia Diodes Inc.) coupled with Keysight's N5242A VNA are used to transmit and receive the THz beam. The frequency extenders used for data collection are coupled through WR 1.5 horn antennas, which have 3 dB beamwidths of 10° and 84% of Gaussicity for transmission and reception of THz signals. Obviously, this system is capable of recording the complex-valued spectral information of the incident wave. Nevertheless, we note that for the proposed *Phaselift* approach, we only use the magnitude of the measured signals.

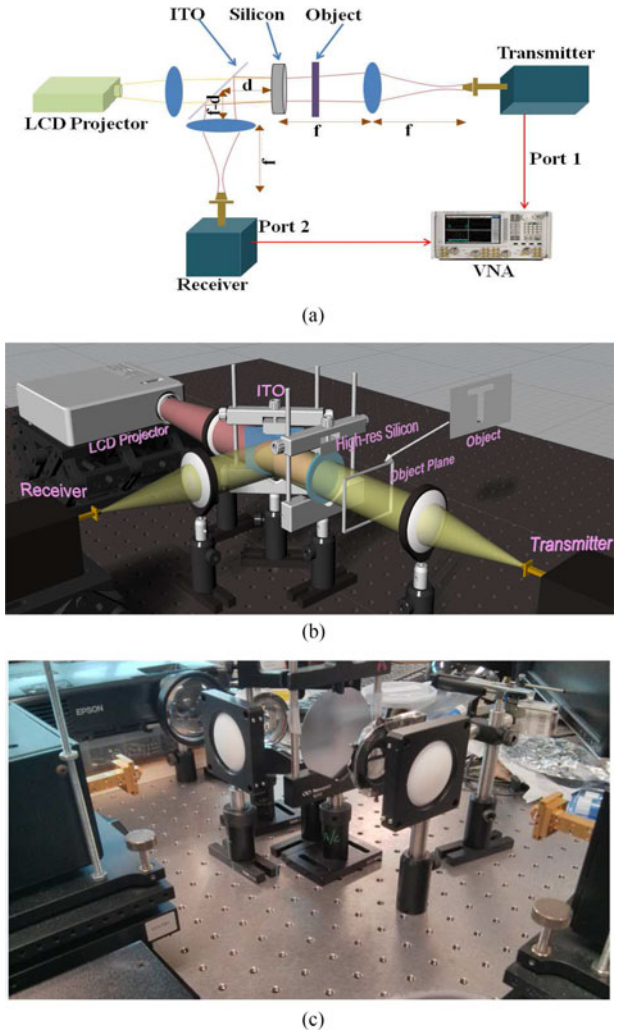

Fig. 4. Experimental setup of the Phaselift compressive THz imaging approach: a collimated THz beam illuminates the scene and the Si wafer forms the complex-valued CS masks. The modulated light is then reflected by an ITO coated glass and focused towards the receiver.

A convex lens is placed in front of the receiver at a distance of 7.5 cm (same as its focal length) to collimate the beam. The high-resistivity Si wafer is placed 7.5 cm away from the lens, where the collimated beam has its beam waist and the wavefront is planar. The object of interest is placed between the wafer and the lens.

After the wafer, an indium tin oxide (ITO) glass is placed at 45° with respect to the THz signal's path to split the optical signal from the THz beam. The ITO film is a conductive glass, which is transparent to optical frequency but acts as a mirror ($\sim$80% reflectivity) to the THz wave. To collect the reflected beam and focus it onto the receiver, another lens is placed between the receiver and the ITO glass. The total distance from the wafer to this lens and the distance from the lens to the detector are both 7.5 cm for the sake of symmetry. As noted above, a commercially available LCD projector is used to generate the mask patterns on the wafer from the backside of the ITO glass. The optical light from the projector travels through the ITO glass to reach the Si wafer surface, where photocarriers get

excited, thus modulating the complex dielectric constant of the material (as summarized in the previous section). This change in dielectric constant causes modulation of the transmitted THz wave. To achieve random modulation of the phase-front, binary mask patterns were generated in MATLAB and projected on a $2 \times 2\,\mathrm{cm}^2$ area on the passivated Si wafer. Light intensity on the wafer was measured to be $1\ \mathrm{W/cm}^2$. However, the diameter of the collimated THz beam on the wafer is approximately 1.5 cm, which essentially limits the maximum possible size of the object plane. The weights of lit and dark pixels are measured as follows: For any arbitrary object placed in the object plane, a complex (magnitude and phase) measurement is taken for a mask pattern in which all the pixels are dark. The complex measurement y_{dark} can be written as

$$y_{\mathrm{dark}} = |y_{\mathrm{dark}}|e^{j\theta_{\mathrm{dark}}} = a_{\mathrm{dark}} \sum_{i=1}^{N^2} x_i \tag{8}$$

where a_{dark} is the weight of the dark pixel. Similarly, for an all-lit mask pattern, the measurement y_{lit} is

$$y_{\mathrm{lit}} = |y_{\mathrm{lit}}|e^{j\theta_{\mathrm{dark}}} = a_{\mathrm{lit}} \sum_{i=1}^{N^2} x_i \tag{9}$$

where a_{lit} is the weight of the lit pixel. Taking the ratio of the above two measurements and taking a_{dark} as reference (i.e., $a_{\mathrm{dark}} = 1\angle 0^\circ$), the weight of the lit pixel a_{dark} can be calculated as

$$a_{\mathrm{lit}} = \frac{|y_{\mathrm{lit}}|}{|y_{\mathrm{dark}}|} e^{j(\theta_{\mathrm{lit}} - \theta_{\mathrm{dark}})}. \tag{10}$$

In our experiment, this value turns out to be $0.1\angle 70^\circ$ in our prototype system.

A LabView (NI LabView 2013 SP1) program controls the projection of patterns on the wafer and the simultaneous acquisition of intensity data from the VNA. Measured data were processed in MATLAB, and using the *Phaselift* algorithm, the amplitude and phase of the image were reconstructed. The image acquisition time is limited by four factors: 1) minority carrier lifetime in the Si wafer; 2) refresh rate of the projector; 3) response time of the detector; and 4) time required for data communication. The carrier lifetime is measured to be 50 μs and the projector refresh rate is 60 Hz. The intermediate frequency bandwidth in the VNA is set to 600 kHz with time averaging of 100 samples. So the effective measurement bandwidth is 6 kHz. Therefore, the time required for each measurement is primarily limited by the refresh rate of the projector in our experiment. However, due to the time needed for the LabView program to communicate with the projector and the VNA, and writing the data into a spreadsheet file, each measurement takes 200 ms, which is much longer than the projector refresh rate (16.67 ms). Replacing the projector with a high-speed DMD chipset by Texas Instruments (DLP7000), which can achieve a speed of 32000 frames per second (fps) for binary patterns, and using more efficient means of data communication, the measurement time for each mask pattern could potentially be reduced to 0.2 ms, resulting in a frame rate of 5 fps for 16×16 pixel images. However, the time required for computation to reconstruct a 16×16 pixel image in MATLAB is approximately 50 s in a computer with an Intel Core i7 3.40 GHz processor and 8 GB memory. So, the total time from the measurement to reconstruction is roughly 6 min for each 16×16 pixel image. To achieve real-time imaging, application-specific integrated circuit implementation of the *Phaselift* process may be necessary. The *Phaselift* code used in this work can be freely obtained from [26].

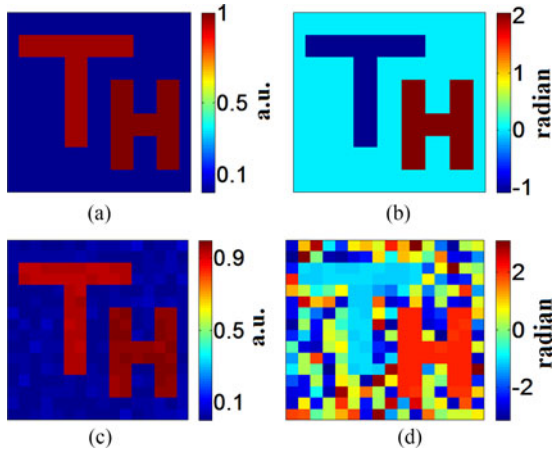

Fig. 5. Reconstruction of a 16×16 pixel phantom image from complex binary mask patterns using *Phaselift*: (a) magnitude of original image, (b) phase of original image, (c) reconstructed magnitude, and (d) reconstructed phase.

V. Experimental Results

As noted above, for an accurate reconstruction of the magnitude and phase of the scene, $\mathrm{O}(n \log n)$ independent measurements are necessary for an $N \times N$ complex image, where $n = N^2$. Random Gaussian amplitude and phase masks yield image reconstruction with a high degree of accuracy, as noted in [20]. However, in the experimental setup discussed above, the amplitude and phase modulation are inherently correlated due to the Drude model of Si photoconductivity. To verify the fidelity of reconstruction with amplitude-phase correlated binary mask measurements, we considered a 16×16 phantom complex image containing the letters "T" and "H" generated in MATLAB, as shown in Fig. 5. Both letters have almost an equal transmission magnitude, but they exhibit substantial contrast in phase, as depicted in Fig. 5(a) and (b). Using 1420 measurements obtained with the aforementioned binary mask patterns (for $n = 256$), the 16×16 complex image can be reconstructed using *Phaselift*, as shown in Fig. 5(c) and (d). As seen in the reconstructed phase in Fig. 5(d), the contrast between the two letters is clearly conserved. The l^2-norm error in the recovery was -24 dB.

With the same set of mask patterns, a 16×16 complex image of an object consisting of thin layers of ordinary printer paper was studied next at 690 GHz. The letter "T" was cut out of 190-μm-thick paper and stacked over another sheet of paper of the same material [see Fig. 6(a)]. We considered this material due to a low absorption (-2 dB) and a refractive index of 690 GHz. As seen in Fig. 6(b), the absorption contrast of the "T"-shaped region is very similar to the background, and thus the letter "T" is barely discernible in the amplitude image.

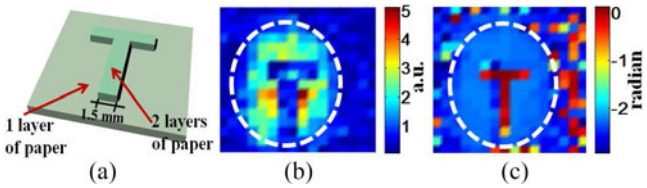

Fig. 6. Illustration of 16×16 phase-sensitive THz imaging using 1420 binary intensity-only measurements and *Phaselift*: (a) "T'-shaped letter made of 190-μm-thick paper stacked over a sheet of paper of the same material, (b) intensity image, and (c) phase image. Each pixel has a dimension of $1.25 \times 1.25\ \text{mm}^2$.

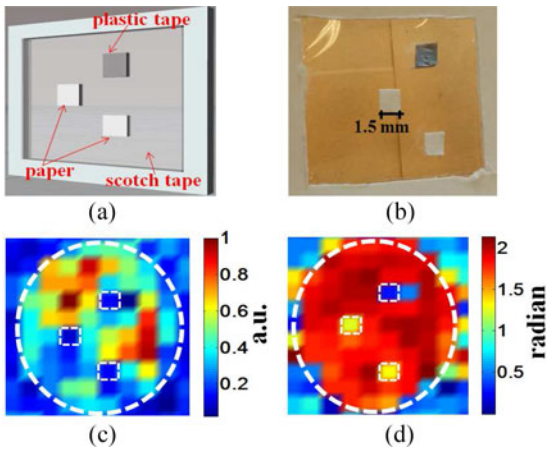

Fig. 7. Illustration 16×16 phase-sensitive imaging using 1420 binary intensity-only measurements and *Phaselift*: (a) three square-shaped objects adhered to a piece of Scotch tape, (b) actual photograph, (c) intensity image, and (d) phase image.

However, the two layers of the paper in the letter "T" provide significant retardation of the phase of the THz signal, producing as much phase difference as 120°. As such, the phase reconstruction via *Phaselift* produces much better contrast and a clearer shape of the image than an intensity image, as demonstrated in Fig. 6(c).

To further illustrate the improved contrast in phase-sensitive THz imaging, we next studied three square-shaped objects, two made of 190-μm-thick paper and one made of plastic tape, all affixed on a piece of thin Scotch tape [see Fig. 7(a) and (b)]. The dimensions of all the square-shaped objects were approximately the size of one pixel ($1.5 \times 1.5\ \text{mm}^2$). The intensity image shown in Fig. 7(c) displays a similar absorption of the three objects and fails to differentiate the difference in the specific materials of each pixel. However, in the phase image shown in Fig. 7(d), the contrast between the paper and the plastic tape objects is clearly visible with the paper objects showing similar phase retardation (shown in yellow). The nonuniformity in phase beyond the beam spot is essentially due to noise.

To further assess the *Phaselift* performance, we next studied the phase reconstruction using complex measurements and CS. We used MATLAB codes of both complex CS and *Phaselift* from [26] for a comparative analysis. A rectangular aperture half covered with one layer of 190 μm-thick paper and the other half covered with two layers of the same material is used as the test case [see Fig. 8(a)]. As noted earlier, our prototype system is capable of recording both the intensity and the phase of the

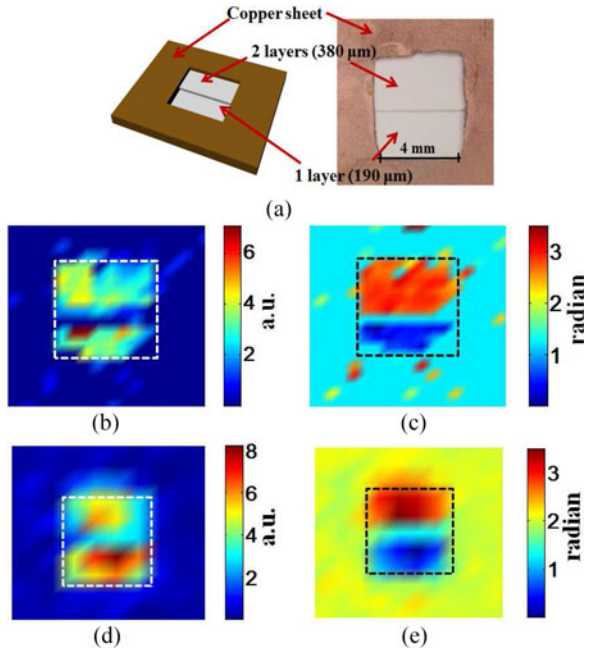

Fig. 8. Comparison of complex CS and *Phaselift* performance: (a) a rectangular aperture half covered with one layer of 190-μm-thick paper and other half covered with two layers of the same paper, (b) 32×32 interpolated intensity image, (c) phase image using 512 complex measurements and a CS algorithm [26], (d) 16×16 interpolated intensity image, and (e) phase image using 1420 intensity-only measurements and the *Phaselift* algorithm.

received signal, allowing us to evaluate complex CS algorithms as well. To compare the two methods, both the intensity and the phase of the modulated wave are recorded for each mask pattern for the complex CS method. For the *Phaselift* reconstruction, we converted the complex measurements into amplitude-only data before applying the *Phaselift* procedure. Thus, complex measurements for 512 random binary mask patterns were used in conjunction with the CS code from [26] to reconstruct a 32×32 complex image of the scene. The magnitude and phase of the reconstructed scene are shown in Fig. 8(b) and (c), respectively. When the same aperture is imaged using a 16×16 *Phaselift* reconstruction with 1420 complex masks and intensity-only measurements, the two methods show comparable intensity and phase profiles, as illustrated in Fig. 8(d) and (e).

VI. Conclusion

We have demonstrated, for the first time, phase-sensitive THz single-pixel imaging using intensity-only measurements and the *Phaselift* algorithm. We employed the photoexcitation of high-resistivity silicon and a commercial LCD projector to implement an optically reconfigurable SLM with "complex" transmission modulation. We show that it is possible to accurately reconstruct both intensity and phase images using intensity-only measurements in the THz band. We have demonstrated superior contrast of phase reconstruction over intensity images using representative examples. In addition, we also compared the performance of the *Phaselift* approach with complex-valued CS reconstruction. Although *Phaselift* requires many more measurements than complex-valued CS, it produces

similar results from intensity-only measurements using only a low-cost power detector. Considering that phase-sensitive detectors are rather costly and add to the overall size and weight of typical THz imaging apparatus, the use of a simple intensity-only detector results in a cost-effective and accurate THz phase-sensitive imaging system. A measurement speed as fast as 0.2 ms/pixel is achievable by using a high-speed DMD chipset for mask projection and a hardware-based implementation of the *Phaselift* procedure, which is much faster than a typical raster scan imager that typically requires 100 ms/pixel scan time. To further speed up the process, compressive phase-retrieval techniques can also be applied to reduce the number of measurements for sparse scenes. De-correlation of amplitude and phase modulation and prevention of heating of the wafer by the incident optical light can further reduce the phase errors in reconstruction.

ACKNOWLEDGEMENTS

The authors would like to thank Prof. T. Strohmer of the University of California, Davis, CA, USA, and Prof. L. C. Potter of The Ohio State University, Columbus, OH, USA, for the discussions regarding the *Phaselift* algorithm.

REFERENCES

[1] L. Rong *et al.*, "Terahertz in-line digital holography of human hepatocellular carcinoma tissue," *Sci. Reports*, vol. 5, no. 8445, p. 6, 2015.
[2] C. Muehleman, J. Li, M. Wernick, J. Brankov, K. Kuettner, and Z. Zhong, "Yes, you can see cartilage with x-rays: Diffraction enhanced x-ray imaging for soft and hard tissues," *J. Musculoskeletal Neuronal Int.*, vol. 4, no. 4, p. 369, 2004.
[3] M. N. Wernick *et al.*, "Multiple-image radiography," *Phys. Med. Biol.*, vol. 48, no. 23, p. 3875, 2003.
[4] M. Brun, F. Formanek, A. Yasuda, M. Sekine, N. Ando, and Y. Eishii, "Terahertz imaging applied to cancer diagnosis," *Phys. Med. Biol.*, vol. 55, no. 16, p. 4615, 2010.
[5] J. F. Federici *et al.*, "THz imaging and sensing for security applications explosives, weapons and drugs," *Semicond. Sci. Technol.*, vol. 20, no. 7, p. S266, 2005.
[6] S. Zhong *et al.*, "Non-destructive quantification of pharmaceutical tablet coatings using terahertz pulsed imaging and optical coherence tomography," *Opt. Lasers Eng.*, vol. 49, no. 3, pp. 361–365, 2011.
[7] G. C. Trichopoulos, H. L. Mosbacker, D. Burdette, and K. Sertel, "A broadband focal plane array camera for real-time THz imaging applications," *IEEE Trans. Antennas Propag.*, vol. 61, no. 4, pp. 1733–1740, Apr. 2013.
[8] B. Hu and M. Nuss, "Imaging with terahertz waves," *Opt. Lett.*, vol. 20, no. 16, pp. 1716–1718, 1995.
[9] D. Takhar *et al.*, "A new compressive imaging camera architecture using optical-domain compression," *Proc. SPIE*, vol. 6065, 2006, Art. no. 606509.
[10] W. L. Chan, H.-T. Chen, A. J. Taylor, I. Brener, M. J. Cich, and D. M. Mittleman, "A spatial light modulator for terahertz beams," *Appl. Phys. Lett.*, vol. 94, no. 21, 2009, Art. no. 213511.
[11] S. Savo, D. Shrekenhamer, and W. J. Padilla, "Liquid crystal metamaterial absorber spatial light modulator for THz applications," *Adv. Opt. Mater.*, vol. 2, no. 3, pp. 275–279, 2014.
[12] Q.-Y. Wen *et al.*, "Graphene based all-optical spatial terahertz modulator," *Sci. Reports*, vol. 4, no. 7409, p. 5, 2014.
[13] M. Van Exter and D. Grischkowsky, "Optical and electronic properties of doped silicon from 0.1 to 2 THz," *Appl. Phys. Lett.*, vol. 56, no. 17, pp. 1694–1696, 1990.
[14] H. Alius and G. Dodel, "Amplitude-, phase-, and frequency modulation of far-infrared radiation by optical excitation of silicon," *Infrared Phys.*, vol. 32, pp. 1–11, 1991.
[15] T. Vogel, G. Dodel, E. Holzhauer, H. Salzmann, and A. Theurer, "High-speed switching of far-infrared radiation by photoionization in a semiconductor," *Appl. Opt.*, vol. 31, no. 3, pp. 329–337, 1992.
[16] M. Shams *et al.*, "Approaching real-time terahertz imaging with photo-induced coded apertures and compressed sensing," *Electron. Lett.*, vol. 50, no. 11, pp. 801–803, 2014.
[17] D. Shrekenhamer, C. M. Watts, and W. J. Padilla, "Terahertz single pixel imaging with an optically controlled dynamic spatial light modulator," *Opt. Exp.*, vol. 21, no. 10, pp. 12 507–12 518, 2013.
[18] A. Kannegulla *et al.*, "Coded-aperture imaging using photo-induced reconfigurable aperture arrays for mapping terahertz beams," *IEEE Trans. THz Sci. Technol.*, vol. 4, no. 3, pp. 321–327, May 2014.
[19] W. L. Chan, K. Charan, D. Takhar, K. F. Kelly, R. G. Baraniuk, and D. M. Mittleman, "A single-pixel terahertz imaging system based on compressed sensing," *Appl. Phys. Lett.*, vol. 93, no. 12, 2008, Art. no. 121105.
[20] E. J. Candes, T. Strohmer, and V. Voroninski, "Phaselift: Exact and stable signal recovery from magnitude measurements via convex programming," *Commun. Pure Appl. Math.*, vol. 66, no. 8, pp. 1241–1274, 2013.
[21] D. L. Donoho, "Compressed sensing," *IEEE Trans. Inf. Theory*, vol. 52, no. 4, pp. 1289–1306, Apr. 2006.
[22] E. J. Candès *et al.*, "Compressive sampling," in *Proc. Int. Congr. Mathematicians*, Madrid, Spain, 2006, vol. 3, pp. 1433–1452.
[23] R. G. Baraniuk, "Compressive sensing," *IEEE Signal Process. Mag.*, vol. 24, no. 4, pp. 118–121, Jul. 2007.
[24] N. W. Ashcroft and N. D. Mermin, *Solid State Physics*. New York, NY, USA: Holt, Rinehart and Winston, 1976.
[25] B. Chhabra, S. Bowden, R. L. Opila, and C. B. Honsberg, "High effective minority carrier lifetime on silicon substrates using quinhydrone-methanol passivation," *Appl. Phys. Lett.*, vol. 96, no. 6, p. 3502, 2010.
[26] M. Iwen, A. Viswanathan, and Y. Wang, *SparsePR: Matlab Software for Sparse Phase Retrieval, v1.0*. (2014). [Online]. Available: https://bitbucket.org/charms/sparsepr

Syed An Nazmus Saqueb (S'11–GS'13) was born on October 3, 1988, in Natore, Bangladesh. He received the B.S. degree in electrical and electronics engineering from Bangladesh University of Engineering and Technology, Dhaka, Bangladesh, in 2012. Currently, he is working toward the Ph.D. degree in electrical and computer engineering at The Ohio State University, Columbus, OH, USA.

He is working as a Graduate Research Associate in the ElectroScience Laboratory, Columbus, OH, USA. His research interests include THz imaging and spectroscopy for biomedical, astronomy, and security applications, quasioptical techniques, and millimeter-wave and THz antenna measurement techniques.

Kubilay Sertel (M'03–SM'07) received the Ph.D. degree from the University of Michigan, Ann Arbor, MI, USA, in 2003.

He is currently an Assistant Professor with the Electrical and Computer Engineering Department, The Ohio State University, Columbus, OH, USA, where he was an Adjunct Professor from 2003 to 2012. He was a Research Scientist with the ElectroScience Laboratory, Columbus. He co-authored *Frequency Domain Hybrid Finite Element Methods in Electromagnetics* (Morgan & Claypool, 2006) and *Integral Equation Methods for Electromagnetics* (SciTech Publishing, 2012), and has authored or co-authored more than 70 journal papers and 250+ conference articles. His current research interests include analysis and design of THz and millimeter-wave sensors, antenna arrays, and on-wafer noncontact metrology systems for device and IC testing as well as spectroscopy techniques for biomedical and nondestructive imaging, ultrawide band low-profile phased arrays for cognitive sensing and opportunistic wireless networks, reconfigurable antennas and arrays, and applied electromagnetic theory and computational electromagnetics, particularly curvilinear fast multipole modeling of hybrid integral equation/finite element systems and resolving large-scale, real-life problems on massively parallel supercomputing platforms.

Dr. Sertel is a Fellow of the Applied Computational Electromagnetics Society and a member of its Board of Directors. He is a member of the IEEE Antennas and Propagation and the Microwave Theory and Techniques Societies. He is an elected member of the International Union for Radio Science Commission B. He is also the Editor-in-Chief for Electronic Publications for the IEEE Antennas and Propagation Society.